Thermal-Aware Tracking for Photovoltaics: Reducing Module Degradation Without Sacrificing Yield

Zeinab Haydous, Robinson Cavieres Abarca, Phillip Hamer, Nathan Chang, Felipe Valencia, and Bram Hoex

***Abstract*—Elevated operating temperatures for photovoltaic modules remain a critical challenge for PV systems, particularly in regions with high irradiance. High temperatures lower efficiency and accelerate module degradation. Single-axis trackers generally rely on algorithms that maximize irradiance capture. To tackle the dual challenge of maximizing production while preventing overheating, we propose a thermal-aware tracking algorithm. The method substantially reduces module temperatures during inverter clipping, a common occurrence in PV systems with high dc/ac ratios. By moderating plane-of-array irradiance (POAI) only when excess power cannot be exported, the algorithm reduces the module temperature without compromising energy yield. Validation using an advanced thermal model that accounts for wind-driven convection and radiative exchange with the sky shows that, under the climatic and operational conditions in Chile, the algorithm performs best when panels are oriented closer to horizontal. Implemented on a solar tracker in northern Chile, the algorithm achieved module temperature reductions of up to 7.7 °C along with decreased UV exposure, enhancing thermal performance without compromising system output and thereby improving efficiency while minimizing degradation.**

***Index Terms*—Field testing, inverter clipping, photovoltaic systems, PV module temperature, single-axis tracking, thermal performance.**

I. Introduction

SINGLE-AXIS trackers outperform fixed-tilt systems by dynamically following the sun, capturing more irradiance and delivering higher annual energy output. To reduce shading losses at low solar angles, backtracking algorithms were introduced and have become the industry standard, with slope-aware adjustments for uneven terrain [1]. More advanced control strategies adapt panel tilt according to prevailing sky conditions, trading strict sun alignment for improved diffuse irradiance capture when direct radiation is limited [1]. This adaptive philosophy is reflected in commercial systems such as NEXTracker's TrueCapture, which dynamically switches between row-to-row shading mitigation and diffuse-oriented tracking to maximize energy yield under variable weather conditions [2]. Academic methods such as adaptive real-time tracking (ARTT) incorporate irradiance, cell temperature, and wind speed in real time, achieving up to 32.7% higher yield than fixed-tilt systems and 7.5% more than conventional single-axis trackers [3].

However, most approaches focus on maximizing irradiance and energy output while neglecting module temperature, a key factor for both short-term efficiency and long-term degradation. Module overheating often coincides with inverter clipping, where irradiance-maximizing strategies continue to expose modules to thermal stress without generating additional net yield. While the severity of thermal effects varies across climates, it is particularly pronounced in hot, arid, and desert environments, where high irradiance coincides with limited convective cooling. This challenge is amplified at higher inverter loading ratios (ILRs), which intensify clipping losses during peak generation and rapid solar ramps [4]. Elevated cell temperatures reduce PV conversion efficiency by around 0.25%–0.30% per °C in modern modules [5], [6] and accelerate material degradation, which typically doubles for every 10 °C due to Arrhenius-type thermally activated ageing processes [7] (see Appendix A for a quantitative analysis).

In real operating conditions of grid-connected utility-scale PV plants, power curtailment is increasingly common, adding thermal stresses that are not addressed by existing tracker control strategies. Curtailment arises from transmission constraints, low demand periods, or grid stability requirements, forcing intentional reductions in ac power output despite high available irradiance [8]. Yet, most commercially deployed tracking algorithms continue to optimize for maximum incident irradiance on the dc side, assuming a near-linear relationship between irradiance and exported ac power. Under curtailment, this assumption fails, as increased irradiance does not result in additional delivered energy [9]. Consequently, modules may operate at elevated temperatures without any corresponding gain in useful output, increasing thermal stress while providing no economic benefit. This limitation motivates the development of control approaches

Received 9 November 2025; revised 21 December 2025; accepted 9 January 2026. This work was supported in part by the Australian Government through the Australian Renewable Energy Agency (ARENA) under Grant TRAC2022/12, in part by the Australian Centre for Advanced Photovoltaics, in part by the Solar Energy Research Center (SERC-Chile) under Grant ANID/FONDAP/1523A0006, in part by the Chilean Economic Development Agency (CORFO) under Grant 17PTECES-75830 for the project "AtaMoSTeC," and in part by the Australian Government Research Training Program Scholarship. *(Corresponding author: Z. Haydous.)*

Zeinab Haydous, Phillip Hamer, Nathan Chang, and Bram Hoex are with the School of Photovoltaic and Renewable Energy Engineering, University of New South Wales, Sydney, NSW 2052, Australia (e-mail: z.haydous@unsw.edu.au).

Robinson Cavieres Abarca is with the School of Photovoltaic and Renewable Energy Engineering, University of New South Wales, Sydney, NSW 2052, Australia, and also with Atamostec Corporation, Antofagasta, Chile (e-mail: r.cavieresabarca@student.unsw.edu.au).

Felipe Valencia is with Atamostec Corporation, Antofagasta, Chile, and also with the Institute of Electricity and Electronics, Faculty of Engineering Sciences, Austral University of Chile, Valdivia, Chile (e-mail: felipe.valencia@atamostec.cl).

Digital Object Identifier 10.1109/JPHOTOV.2026.3654124

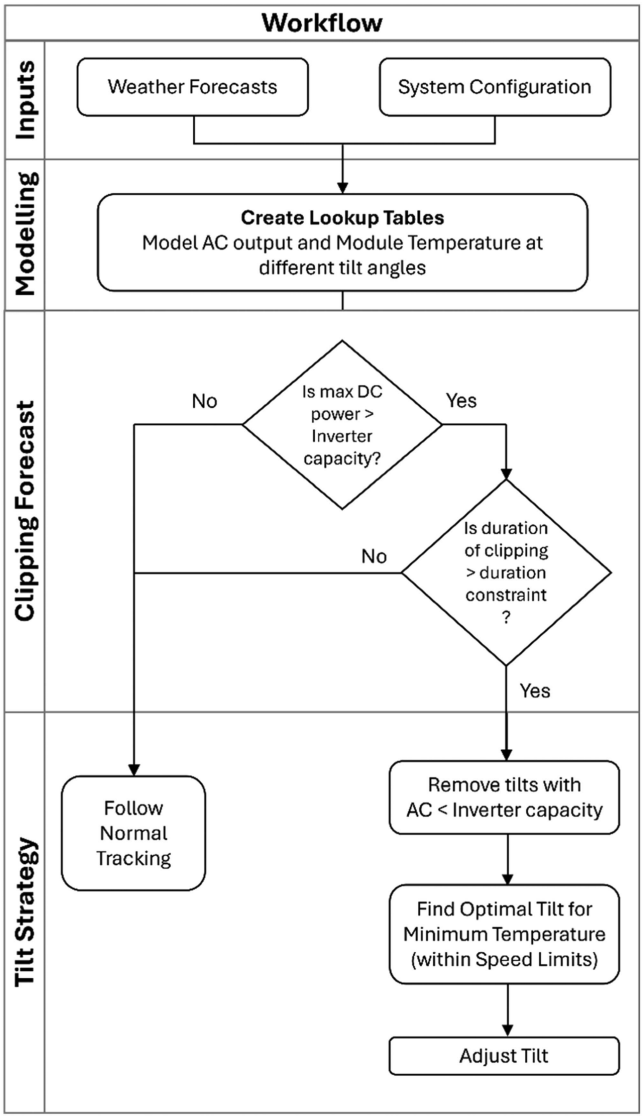

Fig. 1. Workflow for proposed tracking strategy.

that explicitly consider both thermal behavior and export constraints under curtailment conditions.

A thermal-aware tracking algorithm provides a practical solution by reducing module temperatures during nonexportable periods, such as inverter clipping or grid curtailment. By adjusting tracker orientation when additional irradiance cannot be converted into ac energy, the strategy mitigates thermal stress without compromising output and aligns tracker operation with real-world constraints. In this work, we present a proof of concept for thermal-aware tracking for photovoltaics, describing the methodology under clipping conditions—which can be extended to curtailment—and validating its effectiveness through an experimental case study.

II. Methodology

A. Proposed Tracking Strategy

Fig. 1 shows the full workflow of the proposed tracking method, including how clipping is detected and how the optimal tilt is selected. The process begins with weather forecasts and system configuration data, which are used to simulate dc/ac power output and corresponding module temperature across a range of tilt angles. These simulations generate lookup tables that allow the algorithm to evaluate, at each timestep, which tilt angles produce full inverter ac power at the lowest module temperature.

Clipping is then forecasted by comparing the simulated dc power with the inverter limit. If clipping is predicted, the algorithm also checks whether the predicted clipping period exceeds a duration constraint. In this implementation, the duration constraint is defined as a minimum period of sustained clipping (e.g., $>$2 hours). Short clipping events are ignored because the tracker cannot safely reposition and return within such a short window. When clipping is both present and long enough, the algorithm identifies all tilt angles that still deliver the inverter-limited ac output and removes angles below this threshold. It then selects, for each timestep, the tilt angle that gives the lowest module temperature. During this selection, a second constraint is applied: the tracker must respect the actuator speed limit. In this implementation, the speed limit is defined as the maximum permissible change in tilt angle per minute (e.g., 5°/min). Tilt positions that would require motion exceeding this rate when entering or exiting a clipping interval are excluded, ensuring that only angles physically attainable within the actuator's movement capability are considered. If a clipping period does not satisfy the duration constraint, or if all feasible angles violate the speed limit, the tracker defaults to normal tracking for that interval. These steps correspond directly to the workflow illustrated in Fig. 1, progressing from data inputs and simulation through clipping assessment, constraint checks, and final tilt selection.

We simulate power output by first calculating the plane-of-array irradiance (POAI) with transposition models in PVlib. This POAI is then used to estimate module-level power, accounting for shading effects, including inter-row shading through backtracking. The conversion to ac output incorporates the dc/ac ratio, component efficiencies, and system losses. The operating temperature of the photovoltaic module is simulated using the Faiman model [10], widely adopted in tools such as PVSyst, but modified here to explicitly account for radiative heat exchange and the actual operational efficiency, including clipping effects, as implemented in [11].

Fig. 2 provides an example of the proposed strategy in a clear sky day, where during clipping periods, multiple tilt angles can achieve the maximum ac output limited by the inverter. By overlaying both conventional and proposed tilt positions, the figure demonstrates how the algorithm selects optimal tilts that reduce the operating temperature of modules while remaining within the high-power zone.

B. Site and Experimental Setup

Field experiments were conducted by ATAMOSTEC, Chile in June 2025 at PSDA (Plataforma Solar del Desierto de Atacama), located in the Atacama Desert in the Antofagasta, Chile, using a testbench for multiple types of bifacial module technologies designed to replicate real operating conditions.

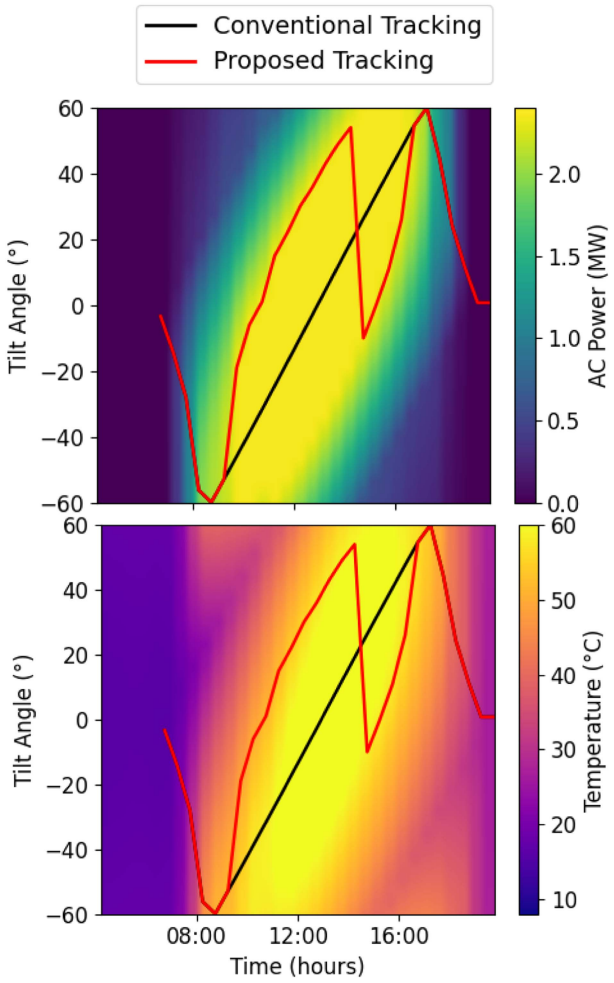

Fig. 2. Heat maps of simulated ac power output and module temperatures across different tilt angles for a clear sky day, with conventional and proposed tracking tilt positions overlaid.

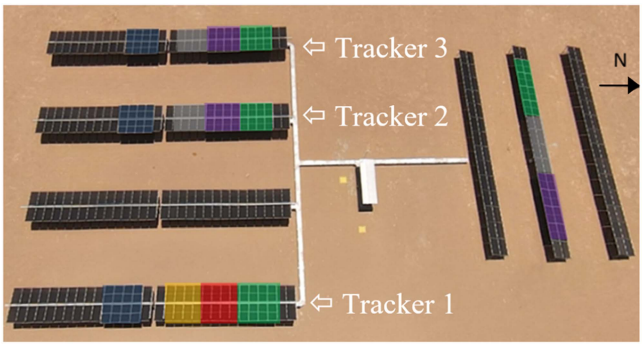

Fig. 3. Aerial view of the solar field in Chile.

The testbench consists of four individual single-axis trackers as shown in Fig. 3. Each highlighted region is a string of eight modules of an individual technology connected in series, while the remaining modules are in open circuit condition, with a total of four strings and 28 dummy modules for Tracker 1, Tracker 2, and Tracker 3. Each tracker is connected to an individual 60 kW inverter with six MPPT inputs, four of which are active, one per technology, totaling 12 kW of installed power per tracker. Each MPPT monitors dc output, while PT100 sensors record module temperature and reference cells on the tracker axis measure front and rear POAI. For environmental monitoring, a weather station records ambient temperature, wind speed, and wind direction. Data from every source is recorded at 1-min intervals.

TABLE I
OPERATIONAL SCENARIOS OF TRACKERS

Tracker	Tracking Algorithm	Clipping Condition
1	Conventional	None
2	Conventional	DC clipping at 6 kW
3	Proposed	DC clipping at 6 kW

Fig. 3 highlights the three trackers selected for this study. Each color represents a different module technology (PERC or HET), with all technologies producing nearly similar power output. Technical details for each module type are provided in Appendix B Temperature measurements reported here correspond to the blue-coded technologies, ensuring comparisons are made between identical module types.

Their operational scenarios are summarized in Table I. Trackers 1 and 2 use conventional single-axis tracking with a horizontal axis, where the ideal tracking angle is based on the Sun's Cartesian coordinates, and backtracking adjusts the position to reduce inter-row shading, following the method in [12]. Tracker 1 provides a baseline under unconstrained conditions. Tracker 2 operates under conventional clipped conditions at 6 kW, while Tracker 3 applies the proposed tracking algorithm. Having identical module technologies in Trackers 2 and 3 facilitates a more accurate comparison of their performance under the same clipping conditions.

The new tracking algorithm is based on conventional single-axis horizontal tracking. Tracker angles are adjusted gradually from the initial position while continuously monitoring power to avoid any reduction in output. Backtracking is maintained to prevent row-to-row shading: In the morning, angles may increase above the conventional position but are never reduced, while in the afternoon, angles either stay at the maximum allowable or decrease to avoid shading and output loss.

To evaluate the effectiveness of the strategy, this work compares two approaches for tilting panels during clipping periods. The first, lead-only, keeps the tracker consistently ahead of the conventional tilt angle. A masking constraint ensures that only tilt positions at or above the standard tracking angle are considered, allowing the tracker to remain in a stable leading posture with minimal movement. The second approach, lead-lag, allows the tracker to move ahead of the sun in the morning and shift to a lagging position in the afternoon. This wider tilt range alters the panel's view of the sky at different times of day, thereby affecting radiative and convective heat exchange. Both strategies were applied on Tracker 3 on different days, with some

days using the lead-only strategy and others using the lead–lag strategy. Both approaches were compared to standard tracking on Tracker 2, representing conventional clipped operation, while Tracker 1 served as a baseline with standard tracking under unconstrained conditions.

III. Results

In this section, we present a comparison of module performance under conventional and thermal-optimized proposed tracking, with the thermal-optimized strategy evaluated using its two approaches: lead-only and lead–lag. We refer to Day 1 as the lead-only day and Day 2 as the lead–lag day. Fig. 3 illustrates the tilt angle, view factor, absorbed solar irradiance, and emitted longwave radiation, capturing the thermal and irradiance dynamics across the various tracking approaches. The view factor represents the portion of the sky dome visible to the module, indicating its potential for radiative heat exchange with the sky. In this context, it specifically describes radiative exchange, not the irradiance-related view factor that considers the sun's position. It can be calculated from the module's tilt using geometric relationships based on Lambert's cosine law, which emphasizes sky regions perpendicular to the module tilted surface [13].

On Day 1, the lead-only algorithm produced steeper afternoon tilts, which reduced the modules' sky view factor and limited radiative cooling, while absorbed irradiance increased. In contrast, on Day 2, the lead–lag strategy maintained tilts closer to horizontal, increasing sky exposure and enhancing radiative heat loss.

The increase in radiative cooling at shallower tilt angles also modulates convective cooling due to the coupling between these heat-transfer mechanisms. This is consistent with the findings by McIntosh et al. [14], who recommended adjusting the convective heat-transfer coefficient based on tilt to account for free-convection effects, reinforcing the observed relationship between tilt and thermal performance. As observed, the mean temperature reduction between Tracker 3 and Tracker 2 increased from 2.74 °C on Day 1 to 3.13 °C on Day 2, confirming the stronger cooling effect of the lead–lag strategy.

In the days presented, Tracker 3 shows a minor increase in absorbed irradiance in the early morning due to slightly steeper tilt angles, possibly enhanced by additional reflected irradiance. This effect highlights the importance of accurate control at the start and end of tilt changes. Tracker 1 does not exhibit a similar increase in the morning, as it is not located at the east edge; an additional tracker positioned east of Tracker 1, not included in the experiment, is noted in Appendix B.

Fig. 5 extends this analysis by presenting the temperature differences across all 11 experimental days, grouped by tracking strategy. During lead–lag periods (middle plot), Tracker 3 consistently operates at lower temperatures than Tracker 2, with pronounced afternoon reductions when the lead–lag behavior reduces absorbed irradiance and increases sky exposure, enhancing radiative cooling. In contrast, during lead-only afternoons, Tracker 3 can be warmer than Tracker 2 primarily because its westernmost position and steeper tilt expose it to higher POAI from direct sunlight in the west and from ground reflections,

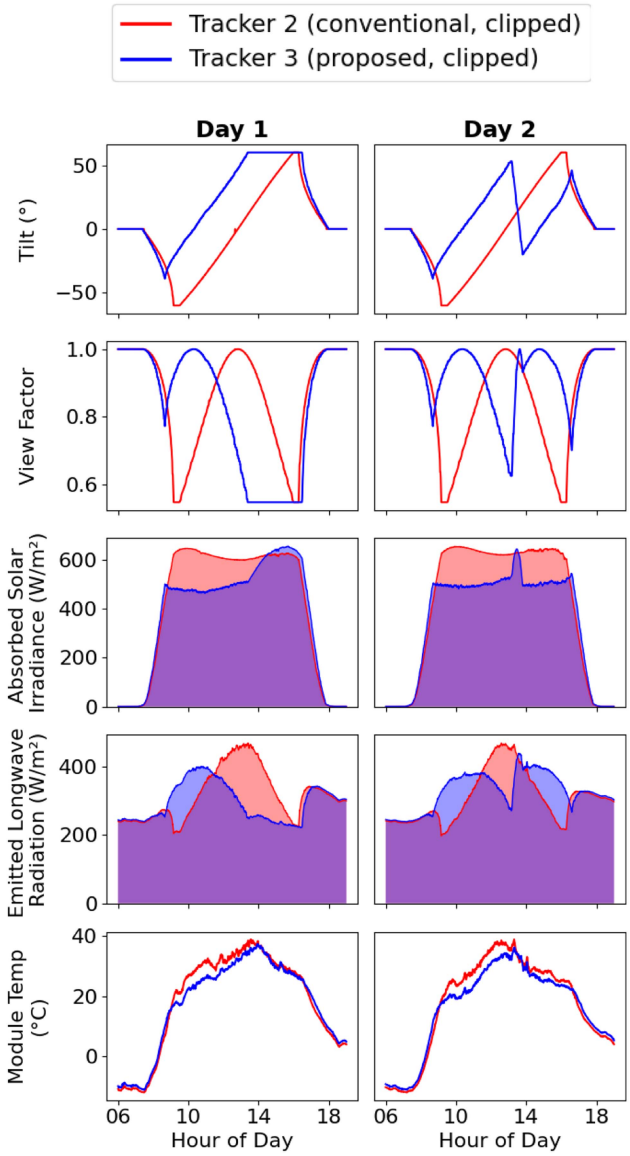

Fig. 4. Comparison of conventional (Tracker 2) and proposed (Tracker 3) tracking strategies over two consecutive days. On Day 1, Tracker 3 follows a continuous lead strategy, while on Day 2, Tracker 3 employs a lead strategy in the morning and a lag strategy in the afternoon.

as reflected by slightly higher absorbed solar irradiance in the afternoon of Day 1 (see Fig. 4). Minor contributing factors include Tracker 2's lower tilts, which enhance radiative cooling, and its movement while Tracker 3 remains at its tilt limit, which can increase local convection and further cool Tracker 2.

The bottom plot of Fig. 5 shows that Tracker 2 generally runs slightly hotter than Tracker 1 due to clipping-related thermal loading. Occasional convergence occurs because prevailing westerly winds (see Fig. 6) provide stronger forced-convection cooling to the westernmost trackers, and Tracker 3's shallower tilt on lead–lag days reduces wind shielding, allowing more airflow to reach Tracker 2. However, comparing the temperature differences between Tracker 2 and Tracker 1 (T2−T1) with those between Tracker 2 and Tracker 3 (T2−T3) shows that T2−T1 remains minimal, whereas the more pronounced cooling of Tracker 3 is primarily due to reduced absorbed irradiance,

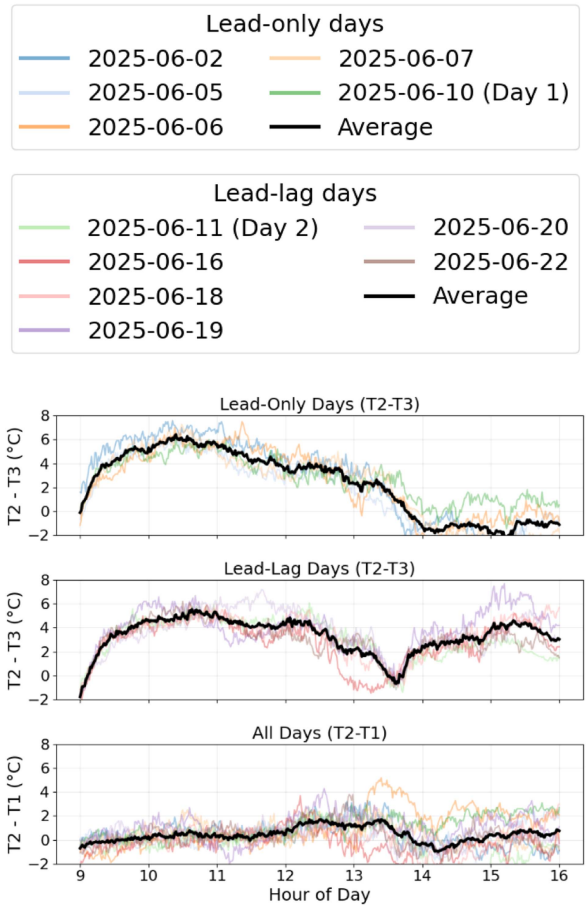

Fig. 5. Temperature differences between trackers: (Tracker 2 − Tracker 3) for lead-only and lead-lag days (top and middle), and (Tracker 2 − Tracker 1) for all days (bottom).

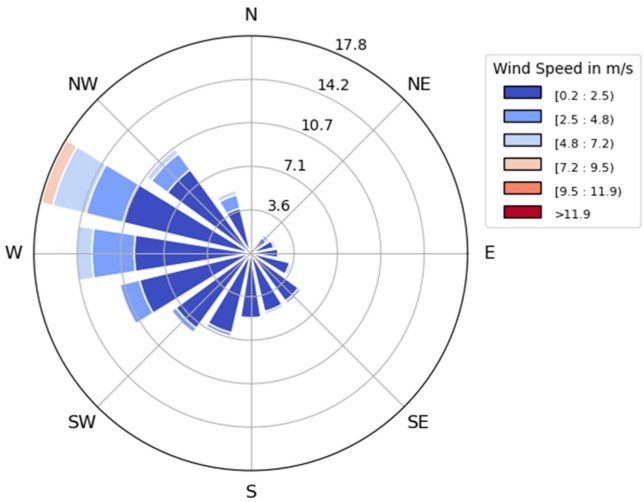

Fig. 6. Windrose from onsite measurements (June 2025).

highlighting the effectiveness of the proposed tracking strategy. These observations suggest that intraday temperature variations arise from thermal loading, local wind effects, and radiative exchange, while the sustained cooling of Tracker 3 is predominantly driven by the tracking method.

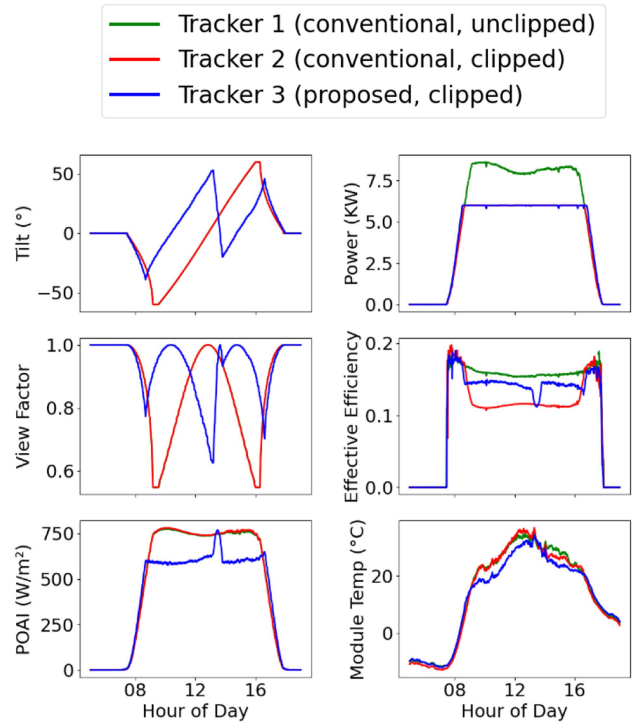

Fig. 7. Performance of the three solar trackers: tilt angle, view factor, POAI, power, effective efficiency, and module temperature.

Fig. 7 shows the detailed operational parameters for each tracker on Day 2, when the lead–lag strategy was applied, arranged to illustrate the cause–and–effect sequence. The plots show that the algorithm limited incident irradiance to regulate output, producing a power curve on Tracker 3 clipped at 6 kW, similar to Tracker 2. The afternoon POAI increase on Tracker 3, as discussed earlier, resulted from its edge position, receiving extra western and ground-reflected irradiance.

The observed temperature differences are closely related to key predictors such as sky view factor, POAI, and photoconversion efficiency. Tracker 3 operated at lower temperatures, demonstrating that its dynamic tilt strategy reduced thermal stress by limiting absorbed solar power and enhancing radiative cooling through increased sky exposure. A higher sky view factor allows the panel to radiate heat more effectively to the sky, thereby contributing to lower module temperatures. At the same time, effective conversion efficiency, defined as the ratio of electrical output at the inverter (Pout) to incident power on the module (Pin), is reduced when inverter clipping limits Pout, causing excess energy to be dissipated as heat in the module. By reducing the input POAI during clipping periods, this ratio is restored, allowing a larger fraction of the incident energy to be converted into electricity rather than heat. This controlled adjustment of POAI not only improves instantaneous performance but also enhances the durability and operational lifetime of both modules and inverters. It should be noted that we expect this effect to be significantly larger in summer, when POAI is higher, than during these experiments which were conducted in winter. Thus, for experimental purposes in winter, we deliberately raised the ILR to amplify module heating, allowing a clearer observation of temperature-related effects.

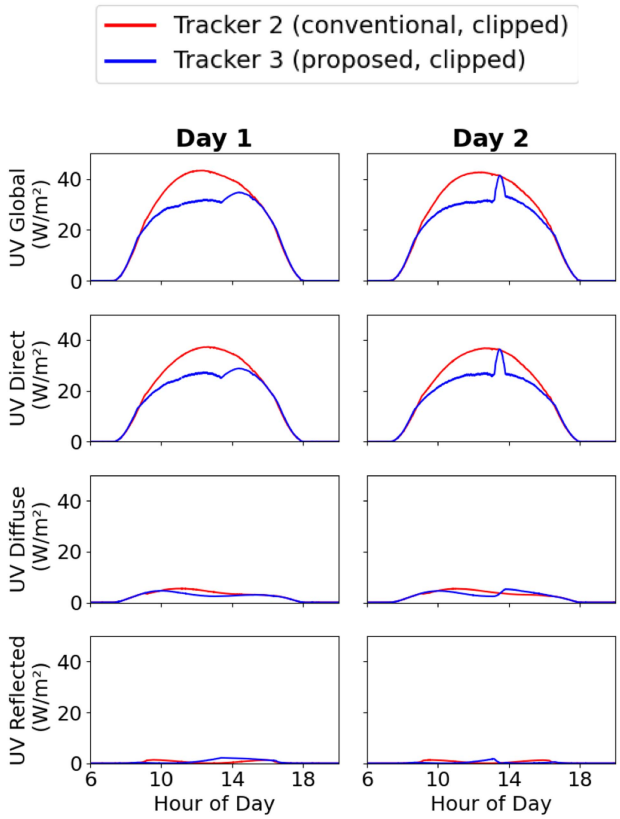

Fig. 8. Hourly UV exposure on the front surfaces of Tracker 2 and Tracker 3 on Day 1 (lead-only strategy) and Day 2 (lead-lag strategy), showing global, direct, diffuse, and reflected components.

Over the full set of 11 simulated days, Tracker 2 reached the highest temperature of 42.7 °C, Tracker 1 peaked at 40.3 °C, and Tracker 3 remained comparatively cooler at 40.9 °C, achieving temperature reductions of up to 7.7 °C. Applying a more aggressive constraint, such as grid curtailment, would likely further increase the temperature differences and corresponding impacts on module efficiency.

Another benefit of the proposed algorithm is the reduction of UV exposure, helping to mitigate thermal stress and UV-induced degradation. Front-surface UV irradiance is calculated from module tilt and solar geometry using a Klucher-based transposition method [15]. As shown in Fig. 8, the algorithm mainly reduces the direct UV component, while diffuse and reflected contributions remain minimal. Implementing the lead-only strategy results in a cumulative global UV reduction of 44 Wh/m^2 on Day 1, whereas the lead–lag strategy achieves higher reductions, reaching 47 Wh/m^2 on Day 2.

These reductions in module temperature and UV exposure have significant implications for long-term durability. Temperature and UV act as primary stressors, affecting chemical reaction rates, diffusion processes, and mechanical fatigue within module materials [7].

By lowering peak temperatures and reducing UV exposure, the algorithm shifts module operation away from the high-stress regions, limiting thermal- and UV-induced degradation. In addition, tilting the array during clipping reduces elevated dc potentials, mitigating the electric fields that drive leakage currents and sodium migration, which contribute to potential-induced degradation (PID).

V. Conclusion

This study introduced a temperature-aware single-axis tracking algorithm designed to minimize module operating temperature and UV exposure while maintaining maximum ac output under clipping conditions. Comparative analysis shows that the lead-only strategy, which kept panels in the leading position relative to conventional tracking, achieved an average temperature reduction of 2.74 °C. The lead–lag approach, tilting panels shallower and closer to horizontal, achieved an average temperature reduction to 3.13 °C, indicating improved cooling performance. Throughout the test period, the thermal-aware tracking algorithm achieved temperature reduction up to 7.7 °C. In addition to lowering module temperatures, the algorithm also reduces UV exposure, particularly the direct component, with cumulative reductions in global UV irradiance of 44 Wh/m^2 on Day 1 (lead-only) and 47 Wh/m^2 on Day 2 (lead–lag), helping to mitigate UV-induced degradation and thermal stress.

It should be noted that, while the algorithm performs well across different sites and weather conditions, its benefits and optimal implementation depend on local climate and site characteristics. Factors such as wind, humidity, cloud cover, altitude, terrain, shading, ambient temperature, and irradiance influence convective and radiative cooling, guiding panel tilt optimization. In high-altitude deserts such as Chile, radiative cooling dominates, and the lead–lag strategy with shallower tilts is favored, though additional tracker movement may increase mechanical stress, requiring careful site-specific operational decisions.

Building on these results, we propose experimental validation of the tracking algorithm alongside further thermal modeling studies, as the thermal behavior at desert sites with high humidity and potential dew or frost events requires deeper analysis. An additional challenge for future work is curtailment, which, driven by market and policy factors such as fixed-price contracts and misaligned pricing structures, presents more complex operational constraints than clipping—for example, in South Australia, nearly 30% of pricing intervals are negative [11]. To address uncertainties such as weather forecast inaccuracies, the algorithm can be applied in a more conservative manner, and future research will evaluate its sensitivity to forecast errors. In addition, research will focus on integrating the algorithm with both clipping and curtailment strategies, performing seasonality analyses, and assessing performance under different ILRs, ensuring robust operation across diverse conditions.

Appendix A
Arrhenius-Based Degradation Analysis

The degradation rate of PV modules can be approximated using an Arrhenius-type model as follows:

$$k\,(T)\ = k_0\, e^{-E_a/(\mathrm{RT})}$$

where

1) $k(T)$ is the degradation rate at temperature T(K);
2) k_0 is a reference rate constant;

3) E_a is the activation energy (J/mol);
4) $\mathrm{R} = 8.314\ \mathrm{J/(mol\backslash K)}$ is the gas constant.

Using a typical activation energy of $E_a = 0.7\,\mathrm{eV} \approx 67540\,\mathrm{J/mol}$, the rate ratio for a 10 °C increase (from 25 °C to 35 °C) is as follows:

$$\frac{k\,(T_2)}{k\,(T_1)} = e^{-E_a/R\cdot(1/T_2 - 1/T_1)} \approx 2.$$

This demonstrates that degradation roughly doubles for every 10 °C increase in module temperature.

Appendix B
Site Details

Fig. 9. Aerial view of the solar tracker layout, highlighting the additional tracker positioned to the east of Tracker 1 (not included in the experiment) and showing that Tracker 3 is centrally located.

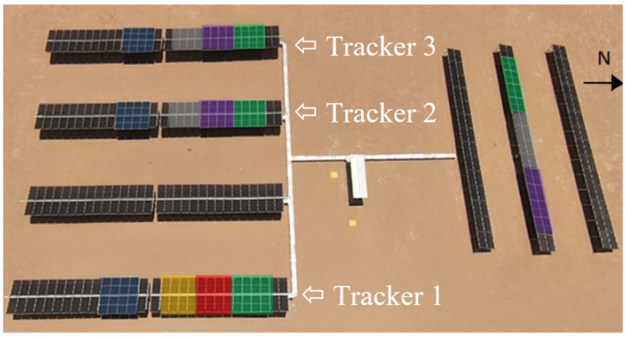

Fig. 10. Aerial view of the solar field in Chile showing color codes.

TABLE II
Summary of Module Technologies, with Colors in Fig. 10 Indicating the Specific Module Type Used in Each Tracker

Color	Tech	Power of Module (W)	Power of String (W)	Bifaciality BF (%)
	PERC+	390	3120	70
	HET	376	3008	90
	HET	375	3000	90
	PERC+	440	3520	70
	HET	380	3040	88
	PERC+	440	3520	70

Acknowledgment

The authors thank Keith McIntosh and Malcolm Abbott for assistance with datasheet modelling and manuscript review, and Thorsten Trupke, Oliver Kunz, and Jürgen Weber for helpful early discussions. The dataset supporting this work is available at https://unsworks.unsw.edu.au/entities/dataset/685d6abd-4ed6-4a65-bdc4-71e77c0bcff9.

References

[1] R. Sadeghi, M. Parenti, S. Memme, M. Fossa, and S. Morchio, "A review and comparative analysis of solar tracking systems," *Energies*, vol. 18, no. 10, Oct. 2025, Art. no. 2553.
[2] D. Shugar, V. Abbaraju, D. Shively, and S. Moskowitz, "PV system performance with single-axis trackers: A GTM executive summary," Nextracker, Fremont, CA, USA, 2018. Accessed: Jan. 21, 2026. [Online]. Available: https://oss.solarbracket.cn/wp-content/uploads/2019/11/NEXTracker_MaximizingPerformance_Single_AxisTrackers.pdf
[3] L. Sun, J. Bai, R. K. Pachauri, and S. Wang, "A horizontal single-axis tracking bracket with an adjustable tilt angle and its adaptive real-time tracking system for bifacial PV modules," *Renew. Energy*, vol. 221, Jan. 2024, Art. no. 119762.
[4] J. Good and J. X. Johnson, "Impact of inverter loading ratio on solar photovoltaic system performance," *Appl. Energy*, vol. 177, pp. 475–486, Sep. 2016.
[5] DAS-Solar, "DAS-DH108ND module datasheet (black frame) –440–460 W," Jan. 2024. Accessed: Jan. 21, 2026. [Online]. Available: https://www.das-solar.com/uploads/20240123EN/Datasheet\%20DAS-DH108ND-EN-440-460(Black\%20Frame).pdf
[6] Rayzon Solar Ltd., "Rayzon TopCon module datasheet 2024 (domestic): 580–600 wp N-type TopCon bifacial (glass-to-glass)," 2024. Accessed: Jan. 21, 2026. [Online]. Available: https://rayzonsolar.com/img/datasheet/Rayzon-Topcon-Datasheet-2024-Domestic.pdf
[7] M. Aghaei et al., "Review of degradation and failure phenomena in photovoltaic modules," *Renewable Sustain. Energy Rev.*, vol. 159, 2022, Art. no. 112160.
[8] M. Laimon, "Renewable energy curtailment: A problem or an opportunity?," *Results Eng.*, vol. 26, 2025, Art. no. 104925.
[9] W. Amnuaypongsa, Y. Suparanonrat, N. Tongamrak, and J. Songsiri, "Estimation of solar panel efficiency in the presence of curtailment," in *Proc. 22nd Int. Conf. Elect. Eng./Electron., Comput., Telecommun. Inf. Technol.*, Bangkok, Thailand, May 2025, pp. 1–6.
[10] Pvlib Python contributors. (n.d.). pvlib.temperature.faiman_rad—pvlib python 0.13.1 documentation. Accessed: Jan. 21, 2026. [Online]. Available: https://pvlibpython.readthedocs.io/en/stable/reference/generated/pvlib.temperature.faiman_rad.html
[11] M. Kim et al., "Accurate modelling of module temperature for ground-mounted PV and its impact on degradation," to be published.
[12] E. Lorenzo, L. Narvarte, and J. Muñoz, "Tracking and back-tracking," *Prog. Photovolt.: Res. Appl.*, vol. 19 no. 6, pp. 747–753, 2011.
[13] D. Ramadhani, Z. Haydous, P. Hamer, M. Kim, and B. Hoex, "Dynamic sky view factor computation for enhanced PV temperature prediction in a terrain-shaded site," in *Proc. Australas. PV Sol. Res. Conf.*, 2025. [Online]. Available: https://apvi.org.au/solar-research-conference/wp-content/uploads/2025/12/51.pdf
[14] K. R. McIntosh et al., "The influence of wind and module tilt on the operating temperature of single-axis trackers," in *Proc. IEEE 49th Photovolt. Specialists Conf.*, Philadelphia, PA, USA, 2022, pp. 1033–1036, doi: 10.1109/PVSC48317.2022.9938577.
[15] S. Poddar, S. Liu, P. Hamer, and B. Hoex, "Closing the UV-induced photodegradation gap through global scale modelling of fixed tilt and tracking photovoltaic systems," *IEEE J. Photovolt.*, 2025.